How to cite: *Angew. Chem. Int. Ed.* **2023**, *62*, e202311625
doi.org/10.1002/anie.202311625

VIP Heterogeneous Catalysis | Very Important Paper

# Selectivity Control in the Direct CO Esterification over Pd@UiO-66: The Pd Location Matters

*Shuaishuai Hu[+], Chenfan Xie[+], Yu-Ping Xu[+], Xuelu Chen, Ming-Liang Gao, He Wang, Weijie Yang,* Zhong-Ning Xu,* Guo-Cong Guo, and Hai-Long Jiang**

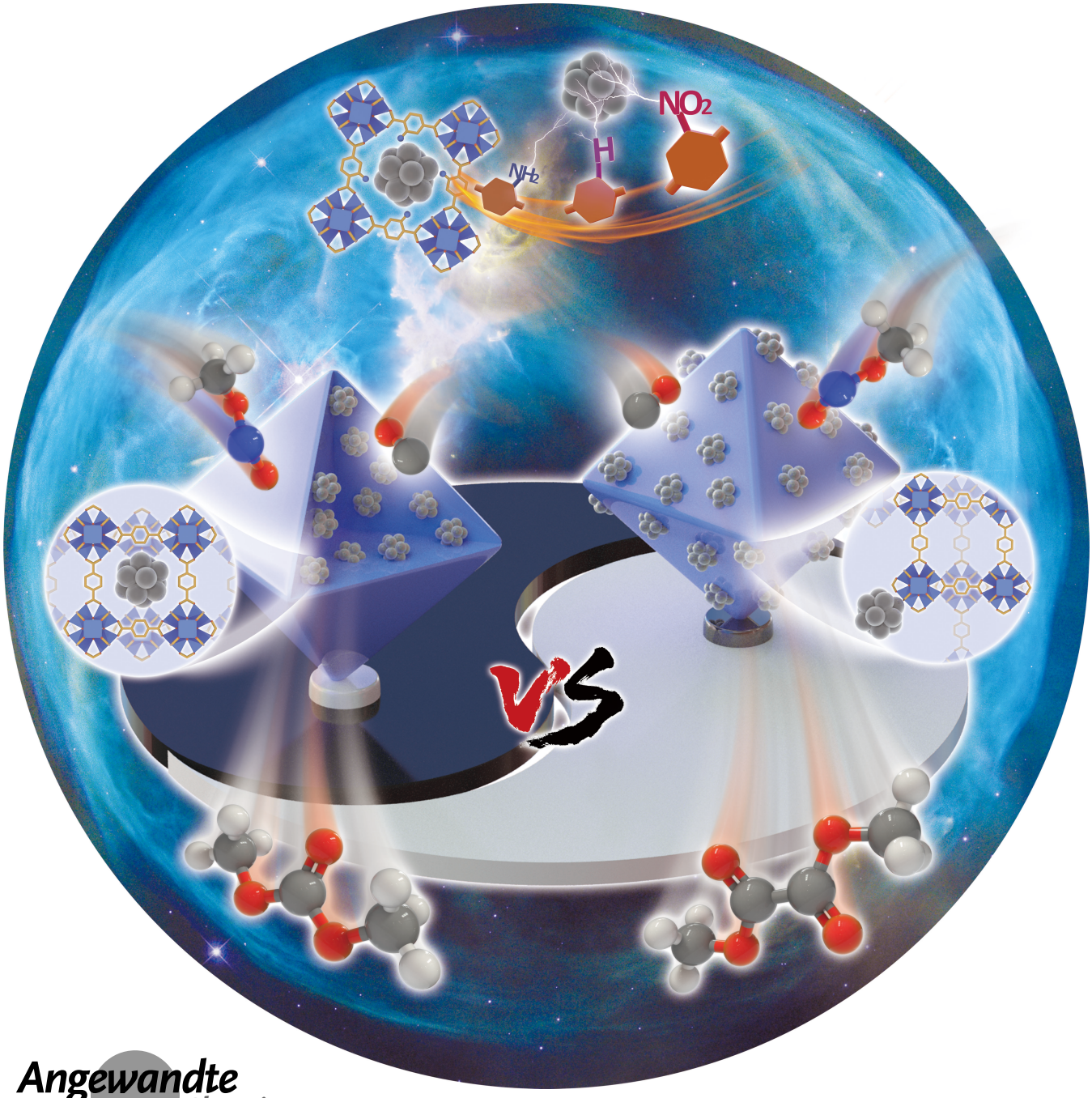


Angewandte International Edition Chemie

**Abstract:** The selectivity control of Pd nanoparticles (NPs) in the direct CO esterification with methyl nitrite toward dimethyl oxalate (DMO) or dimethyl carbonate (DMC) remains a grand challenge. Herein, Pd NPs are incorporated into isoreticular metal–organic frameworks (MOFs), namely UiO-66-X (X=-H, -$NO_2$, -$NH_2$), affording Pd@UiO-66-X, which unexpectedly exhibit high selectivity (up to 99%) to DMC and regulated activity in the direct CO esterification. In sharp contrast, the Pd NPs supported on the MOF, yielding Pd/UiO-66, displays high selectivity (89%) to DMO as always reported with Pd NPs. Both experimental and DFT calculation results prove that the Pd location relative to UiO-66 gives rise to discriminated microenvironment of different amounts of interface between Zr-oxo clusters and Pd NPs in Pd@UiO-66 and Pd/UiO-66, resulting in their distinctly different selectivity. This is an unprecedented finding on the production of DMC by Pd NPs, which was previously achieved by Pd(II) only, in the direct CO esterification.

## Introduction

The direct catalytic conversion of C1 raw materials, such as CO and $CO_2$, to high value-added products is of great importance, offering a promising route to alleviate the growing energy and environmental issues.[1] The direct CO esterification reaction with methyl nitrite, a promising C1 chemical conversion, produces dimethyl carbonate (DMC) and dimethyl oxalate (DMO), which have been widely used to synthesize numerous industrial products.[2] It is recognized that Pd-based catalysts are efficient for the reaction.[3] There have been reported that single-site Pd catalysts and Pd nanoparticles (NPs) are favorable to produce DMC and DMO, respectively.[3b] Nevertheless, the single-site Pd species is easily reduced and aggregated to Pd NPs under the strong reducing CO atmosphere at elevated temperature, giving rise to reduced DMC selectivity.[4] Meanwhile, the supported Pd NPs usually suffer from agglomeration at high reaction temperatures, resulting in a decreased activity.[5] In addition, despite significant research progress in the direct CO esterification, the selectivity control and structure–activity relationship in this conversion are challenging issues, and accordingly related reaction mechanism of CO activation remains controversial. To address the above challenges, it would be of great importance to find suitable supports with well-defined and atomically tailorable structures for Pd NPs.

On this ground, metal–organic frameworks (MOFs), an emerging class of crystalline porous materials constructed by metal ions/clusters and organic linkers, featuring high porosity and ease of structural tailorability, would be promising supports.[6] MOFs have been recognized to be ideal in the incorporation of metal NPs for enhanced catalysis and the pore confinement for metal NPs are favorable to their stability.[7] Moreover, the readily engineered pore walls of MOFs offer congenital advantages to modulate the chemical microenvironment around the confined metal NPs for regulated activity and selectivity.[8] Therefore, incorporating Pd NPs into MOFs with precisely functionalized pore walls would be desired for improving the direct CO esterification and also ideal models for understanding the relationship between structure and performance.

With the above in mind, the representative isoreticular MOFs, UiO-66-X, featuring altered groups on the linker, have been adopted to encapsulate Pd NPs, affording Pd@UiO-66-X (X=-H, -$NO_2$, -$NH_2$). As a control, Pd NPs are supported on UiO-66 to yield Pd/UiO-66. Unexpectedly, it is found that the selectivity of the direct CO esterification with methyl nitrite (MN) over the above Pd catalysts is dominated by the location of Pd NPs. To our surprise, the Pd@UiO-66-X exhibit very high selectivity (81–99%) to DMC in this reaction, which has never been reported for Pd NPs. In contrast, the Pd/UiO-66 tends to produce DMO, a common product over Pd NPs, with selectivity of >89%. Moreover, the Pd electronic state can be modulated by the -X functional group in Pd@UiO-66-X, leading to the optimized activity (Scheme 1). The in situ diffuse reflectance infrared Fourier transform (DRIFT) spectra and density-functional theory (DFT) calculations support that the location of Pd NPs relative to the MOF gives rise to their different levels of interface contact and discriminated microenvironment of Pd NPs, accounting for the distinctly different reaction selectivity. To the best of our knowledge, this is the first finding that the location of Pd NPs relative to the support dominates the product selectivity in the direct CO esterification.

## Results and Discussion

The UiO-66-X, formulated $Zr_6O_4(OH)_4(BDC\text{-}X)_6$ (BDC= benzene-1,4-dicarboxylate, X=-H, -$NO_2$, -$NH_2$), were con-

[*] S. Hu,[+] C. Xie,[+] Dr. M.-L. Gao, H. Wang, Prof. Dr. H.-L. Jiang
Hefei National Research Center for Physical Sciences at the Microscale, Department of Chemistry, University of Science and Technology of China
Hefei, Anhui 230026 (P. R. China)
E-mail: jianglab@ustc.edu.cn
Homepage: http://mof.ustc.edu.cn/
Y.-P. Xu,[+] Prof. Dr. Z.-N. Xu, Prof. Dr. G.-C. Guo
State Key Laboratory of Structural Chemistry, Fujian Institute of Research on the Structural of Matter, Chinese Academy of Sciences
Fuzhou, Fujian 35000 (P. R. China)
E-mail: znxu@fjirsm.ac.cn
X. Chen, Prof. Dr. W. Yang
School of Energy and Power Engineering, North China Electric Power University
Baoding, Hebei 071003 (P. R. China)
E-mail: yangwj@ncepu.edu.cn
Y.-P. Xu[+]
University of Chinese Academy of Sciences
Beijing 100049 (P. R. China)
[+] These authors contributed equally to this work.

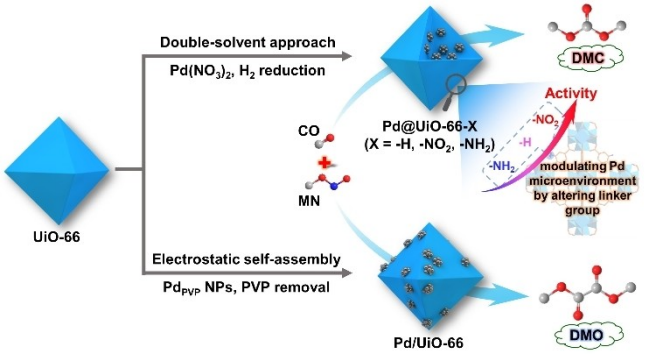


***Scheme 1.*** Schematic diagram for different conversion and selectivity in the direct CO esterification with MN over Pd@UiO-66-X (X=-H, -$NO_2$, -$NH_2$) and Pd/UiO-66.

structed by BDC-X and $ZrCl_4$ by the solvothermal method.[9] The Pd NPs were generated in UiO-66-X by introducing $Pd(NO_3)_2$ into the MOF pores based on the double-solvent approach (DSA) and subsequently reduced by $H_2$, affording Pd@UiO-66-X with similar Pd loadings (0.9–1.1 wt%) (Table S1). In addition, Pd/UiO-66, aiming to assure that all Pd NPs are on the external surface of the MOF, was prepared as a control (Scheme S1). Specifically, the pre-synthesized $Pd_{PVP}$ NPs of ~3.5 nm (Figure S1a), coating with poly(vinylpyrrolidone) (PVP), were assembled with UiO-66 based on electrostatic interaction (Figure S1b), followed by PVP removal in Meerwein's salt solution to yield Pd/UiO-66 with Pd loading of 0.94 wt% (Table S1).[10]

The phase purity and crystallinity of Pd@UiO-66-X and Pd/UiO-66 are confirmed by powder X-ray diffraction (XRD) (Figure S2). Scanning electron microscopy (SEM) images display the typical octahedral morphology and good dispersion of Pd@UiO-66-X and Pd/UiO-66 (Figure S3). The slightly decreased BET surface areas of Pd@UiO-66-X compared with their parent MOF might be due to the increased mass from Pd and/or the pore-blockage effect of Pd,[8a,11] and the BET surface area displays very slight increase from $Pd_{PVP}$/UiO-66 to Pd/UiO-66 by removing PVP (Figure S4).[10a] Transmission electron microscopy (TEM) images verify that Pd NPs with similar sizes of 2–4 nm are dispersed uniformly by the MOF stabilization (Figure S5). Meanwhile, high-angle annular dark-field scanning transmission electron microscopy (HAADF-STEM) image of Pd@UiO-66 demonstrates the absence of obvious Pd NPs on the MOF surface (Figures 1a, S6), and the corresponding elemental mapping results indicate the uniformly dispersed Pd species in Pd@UiO-66 (Figure 1b–d), implying that Pd NPs stay only inside the MOF particle. By contrast, Pd NPs can be clearly observed at the edge of the Pd/UiO-66 particle in its HAADF-STEM image and the corresponding elemental mapping further supports the presence of Pd NPs outside the MOF particle (Figures 1e–h, S7).

To further confirm the location of Pd NPs in Pd@UiO-66 and Pd/UiO-66, the TEM images of their cross-section observation are obtained by slicing up the resin-embedded particles (Figure 1i), which was developed by us for demonstrating the location of metal NPs in the composites

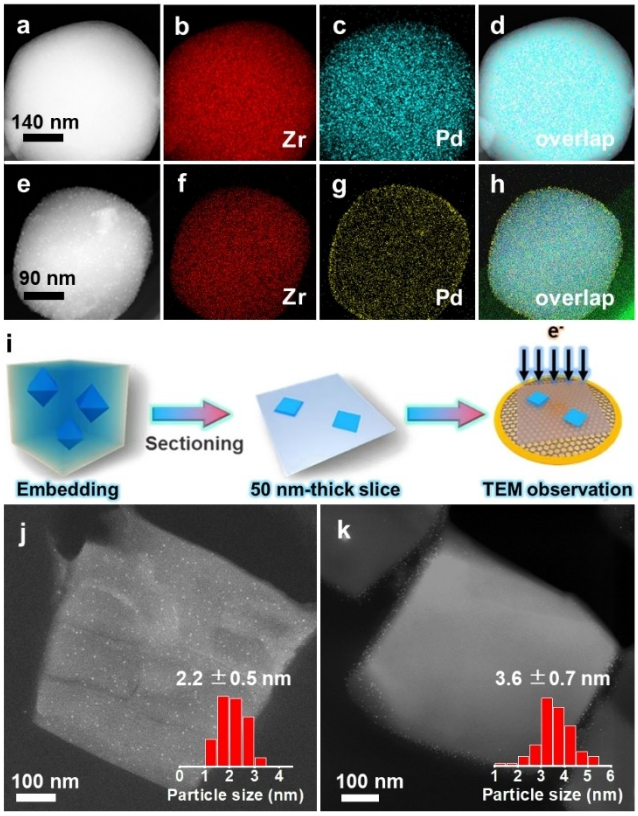


***Figure 1.*** a) HAADF-STEM image of Pd@UiO-66, and b–d) the corresponding elemental mapping of Zr, Pd, and the overlapping elemental mapping of Zr, Pd, C, O. e) HAADF-STEM image of Pd/UiO-66, and f–h) the corresponding elemental mapping of Zr, Pd, and the overlapping elemental mapping of Zr, Pd, C, O. i) Scheme showing the slicing up of resin-embedded Pd@UiO-66 particle by using a diamond knife. HAADF-STEM images of j) sliced Pd@UiO-66 and k) sliced Pd/UiO-66 (insets: size distribution of Pd NPs).

recently.[8b,12] Moreover, the HAADF-STEM image of the sliced Pd@UiO-66 suggests that Pd NPs are uniformly dispersed in the cross-section of the particle, unambiguously verifying that Pd NPs are entirely encapsulated inside the MOF (Figure 1j). In comparison, Pd NPs are merely located at the edge of the cross-section of Pd/UiO-66 particle, demonstrating that Pd NPs are all on the MOF surface (Figure 1k). All the above results jointly support the successful synthesis of Pd@UiO-66 and Pd/UiO-66 with the specific Pd locations.

Encouraged by the successful synthesis, we then set up to explore their catalytic performance toward the direct CO esterification reaction with methyl nitrite (MN). Under the specific reaction condition beneficial to produce DMO (Figure 2, Table S2),[5a,13] negligible product can be detected in the presence of UiO-66 (Table S2, entry 1). Nevertheless, the conversion reaches ~50% for Pd@UiO-66, which identifies Pd NPs as the reactive species in this reaction (Table S2, entry 2). It is astonishing to find that Pd@UiO-66 exhibits high selectivity (~96%) to DMC while low selectivity (~4%) to DMO; on the contrary, Pd/UiO-66 presents high selectivity (~89%) to DMO under the same

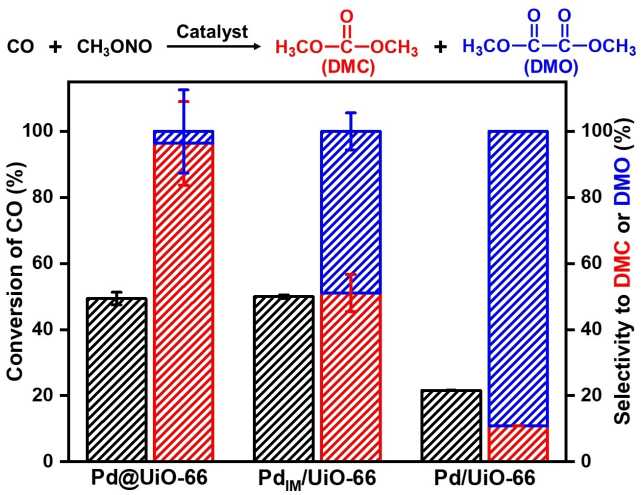


***Figure 2.*** The conversion of CO and product selectivity to DMC or DMO in the direct CO esterification over Pd@UiO-66, $Pd_{IM}$/UiO-66, and Pd/UiO-66. The selectivity and conversion are calculated based on CO. Reaction condition: 180 mg catalyst, 130 °C, 0.1 MPa, weight hour space velocity (WHSV) = 3000 L $kg_{cat.}^{-1}$ $h^{-1}$, reactant gases are composed of 28 % CO, 18 % MN, 4 % Ar, and 50 % $N_2$.

condition (Table S2, entry 3). Given the only difference between Pd@UiO-66 and Pd/UiO-66 lies in the Pd location relative to the MOF particle, the above results imply that the Pd location might play a key role in the selectivity. This is distinctly different from the reported Pd NPs for the direct CO esterification, all of which give very high selectivity to DMO (Table S3). To further verify this result, the $Pd_{IM}$/UiO-66 with similar Pd loading and sizes was fabricated by impregnation method (Figure S8a), where Pd NPs in ~4.7 nm sizes are randomly deposited in the MOF pores and on the MOF surface. The resulting $Pd_{IM}$/UiO-66 produces mixture with 51 % DMC and 49 % DMO (Table S2, entry 4), which might result from the mixed Pd locations. In addition, $Pd/ZrO_2$ was also synthesized as a control (Figure S8b), and it gives high DMO selectivity (~90 %, Table S2, entry 5), very similar to that of Pd/UiO-66, in agreement with the previously reported results (Table S3). The stability investigation suggests that the selectivity to DMC over Pd@UiO-66 shows a slight decrease and reaches a plateau at ~63 % eventually, whereas Pd/UiO-66 displays extremely stable activity and selectivity to DMO during the reaction (Figure S9). The crystallinity, structural stability and Pd sizes of both catalysts are not changed after reaction, as confirmed by powder XRD and TEM results (Figures S10, S11).

The above catalytic results reveal that the Pd location relative to the MOF particle dominates the resulting selectivity. This is an unprecedented finding on the good selectivity to DMO over Pd NPs by incorporating them into a MOF, possibly due to the fact that all reported Pd NPs were on the external surface of diverse supports. To gain deep insight into how the location of Pd NPs affects product selectivity, the processes of oxidative addition and reductive elimination involved in the CO esterification reaction, which lead to a common Pd(0)/Pd(II) cycle,[13,14] have been carefully studied. The Pd 3d XPS spectra of as-synthesized Pd@UiO-66 and Pd/UiO-66 display the binding energy of Pd $3d_{5/2}$ at 335.8 and 335.7 eV, respectively (Figures S12a, S13a), supporting the presence of Pd(0). Two new peaks of 337.5 and 337.3 eV assigned to Pd(II) are observed when both catalysts are treated with MN (Figures S12b, S13b), reflecting that a part of Pd(0) is oxidized to Pd(II) by MN. These two new peaks disappear after treating the catalysts with CO and MN (Figures S12c, S13c), manifesting the occurrence of reductive elimination process.[14]

It is assumed that the Lewis acid sites in MOFs may pose crucial influence on the reaction selectivity based on previous studies.[15] Given the Zr-oxo clusters in UiO-66 give Lewis acid sites, when Pd NPs are incorporated in MOF pores, the interfaces between Pd and Zr-oxo clusters would be very rich. In contrast, when Pd NPs are on the outer surface of UiO-66, the interfaces should be much less between Pd and Zr-oxo clusters.[16] Therefore, the reversed reaction selectivity might be due to the specific microenvironment (with different levels of interface between Pd NPs and Lewis acid sites) surrounding Pd NPs.

To prove the role of Lewis acid sites in UiO-66 in the reaction, in situ DRIFT spectra of UiO-66 have been collected by treating with MN and CO and then purging with Ar gas (Figure S14). When UiO-66 is treated with MN and CO, two peaks at 1033 and 1045 $cm^{-1}$ appear gradually, which are assignable to the $*OCH_3$ intermediate species (Figure S14a).[17] These two peaks exist even after purging with Ar gas for 40 min (Figure S14b), demonstrating that the Lewis acid sites could activate MN and stabilize the $*OCH_3$ intermediate species. The two peaks are also observed with Pd@UiO-66 and Pd/UiO-66 (Figure 3), implying that the two catalysts experience similar intermediate processes. In addition, no peak at approximately 1209 $cm^{-1}$ can be observed on UiO-66, reflecting that the $*COOCH_3$ intermediate species is not generated, which suggests that the Lewis acid sites are not able to produce $*COOCH_3$ intermediate (Figure S14). By contrast, when Pd NPs are present, the signal of $*COOCH_3$ intermediate can be observed with both Pd@UiO-66 and Pd/UiO-66 (Figure 3), demonstrating that Pd NPs are the active sites for producing the $*COOCH_3$ intermediate.

Inspired by the above XPS and in situ DRIFT spectra results, a plausible mechanism can be proposed to illustrate the high DMC selectivity of Pd@UiO-66 and DMO selectivity of Pd/UiO-66 (Figure 4a). First, CO molecules are preferentially adsorbed on Pd NPs, followed by the adsorption of MN molecules on Pd NPs, generating the Pd-NO and Pd-$OCH_3$ intermediates. The NO* species may desorb from Pd NPs directly,[13a] then CO molecules will immediately insert into Pd-$OCH_3$ to form the Pd-$COOCH_3$ intermediate. After that, two different coupling pathways for the intermediates might take place (Figure 4a): 1) For Pd@UiO-66, given the presence of rich interface between Pd NPs and Zr-oxo clusters, Pd NPs are in a microenvironment surrounding with abundant Lewis acid sites (from Zr-oxo clusters) that could activate MN molecules and stabilize the $*OCH_3$ intermediates to form Zr-oxo-$OCH_3$, then one Zr-oxo-$OCH_3$ and one Pd-$COOCH_3$ would couple to yield DMC; 2) For Pd/UiO-66, given the lack of sufficient Lewis

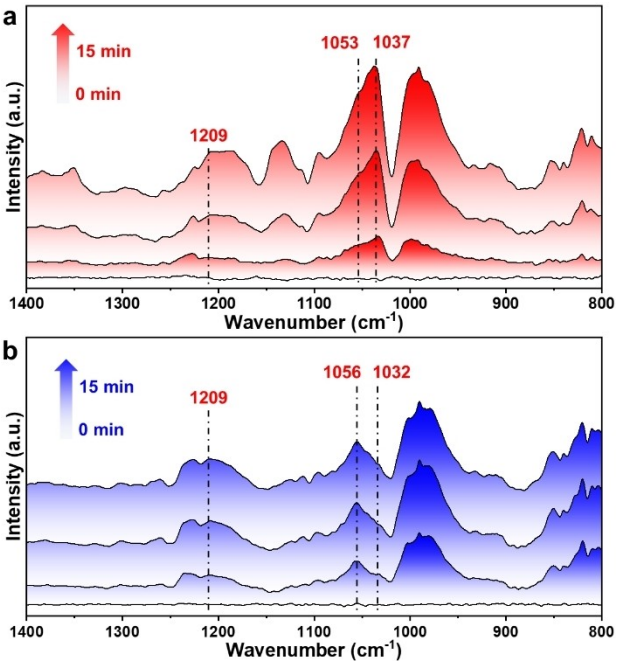


***Figure 3.*** a) In situ DRIFT spectra of Pd@UiO-66 under simulated reaction condition tending to produce DMC: 30 mg catalyst, 120 °C, 0.1 MPa, gas flow rate of 25 mL/min, reactant gases composed of 19 % CO, 45 % MN, 3 % Ar, and 33 % $N_2$. b) In situ DRIFT spectra of Pd/UiO-66 under simulated reaction condition tending to produce DMO: 30 mg catalyst, 130 °C, 0.1 MPa, gas flow rate of 25 mL/min, reactant gases composed of 28 % CO, 18 % MN, 4 % Ar, and 50 % $N_2$.

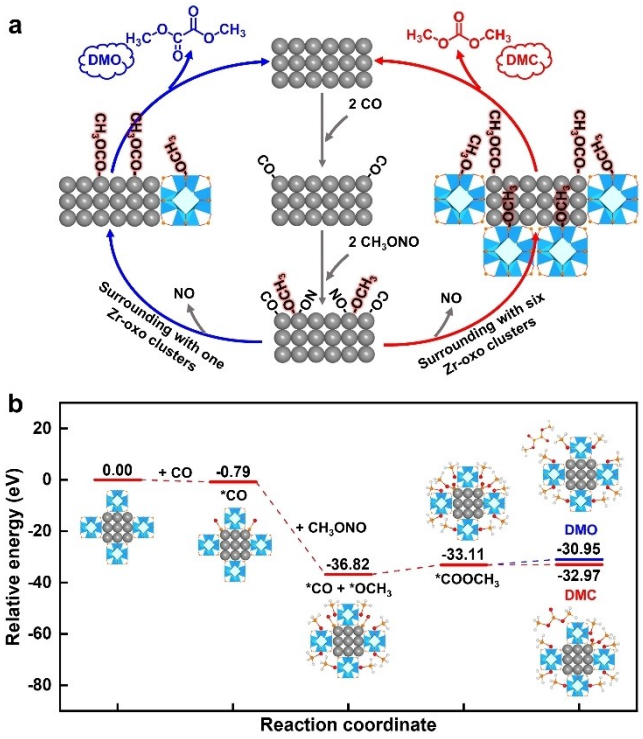


***Figure 4.*** a) The proposed catalytic mechanism of the direct CO esterification reaction with selectivity to DMC (represented by grey and red arrows) and DMO (represented by grey and blue arrows), respectively. b) The calculated relative energies in potential pathways for the direct CO esterification reaction over Pd@UiO-66.

acid sites around Pd NPs due to the limited interface contact, the coupling between two Pd-$COOCH_3$ intermediates would more likely take place, leading to DMO product. The different pathways over Pd@UiO-66 and Pd/UiO-66 are responsible for their distinctly different product selectivity.

To verify the mechanism proposed above, DFT calculations have been adopted to evaluate the relative energy of the direct CO esterification reaction over Pd@UiO-66 and Pd/UiO-66. Given the more interfaces between Pd and Zr-oxo clusters in Pd@UiO-66 than that in Pd/UiO-66, two models, in which Pd NPs surrounding with six and one Zr-oxo cluster respectively correlates with Pd@UiO-66 and Pd/UiO-66, have been constructed and optimized. It is clear that CO is preferentially adsorbed on Pd (−2.29 eV) compared with MN (−0.51 eV), and MN is adsorbed and activated more easily on Zr-oxo clusters (−3.16 eV) than Pd NPs (−0.51 eV) (Figure S15). Therefore, the reaction process is that the adsorption of CO followed by MN takes place on Pd NPs, then CO inserts into Pd-$OCH_3$ to give Pd-$COOCH_3$ intermediate. The relative energy for this step is much different on Pd@UiO-66 (3.71 eV, Figure 4b) and Pd/UiO-66 (−3.82 eV, Figure S16), which imply that the formation of Pd-$COOCH_3$ intermediate is more difficult on Pd@UiO-66 than Pd/UiO-66, giving rise to the less number of Pd-$COOCH_3$ intermediate on the Pd@UiO-66 than Pd/UiO-66. Subsequently, for Pd@UiO-66, the relative energies for the two Pd-$COOCH_3$ intermediates to generate DMO and one Pd-$COOCH_3$ coupling with one Zr-oxo-$OCH_3$ intermediate to afford DMC are 2.16 and 0.14 eV, respectively. This well explains that the Pd-$COOCH_3$ intermediate is prone to couple with one of abundant Zr-oxo-$OCH_3$ intermediates to form the DMC over Pd@UiO-66, rather couple with another Pd-$COOCH_3$ intermediate to DMO. By contrast, the relative energies of generating DMO and DMC are 0.19 and 2.73 eV, respectively for Pd/UiO-66. Therefore, the CO esterification over Pd@UiO-66 is favorable to DMC with high selectivity, while it tends to generate DMO on Pd/UiO-66. From the above results, the different amounts of interface between Pd NPs and Zr-oxo clusters in Pd@UiO-66 and Pd/UiO-66 gives rise to the discriminated Lewis acid microenvironment created by Zr-oxo clusters surrounding Pd NPs, which is able to regulate the selectivity of the direct CO esterification reaction.

To further explore the influence of the MOF functional group on the catalytic performance, Pd@UiO-66-X (X=-H, -$NO_2$, -$NH_2$) have been also examined under the specific reaction condition that favors DMC production in the direct CO esterification reaction (Figure 5a).[5a,13] As expected, all Pd@UiO-66-X with diverse functional groups exhibit high selectivity to DMC (81–99 %). Strikingly, the conversion of CO over the three catalysts follows the order of Pd@UiO-66-$NH_2$ < Pd@UiO-66 < Pd@UiO-66-$NO_2$. To understand the mechanism how different functional groups in Pd@UiO-66-X affect their catalytic activity, the Bader charge by DFT calculations has been evaluated. Results elucidate the corresponding surface electronic states of Pd NPs and the

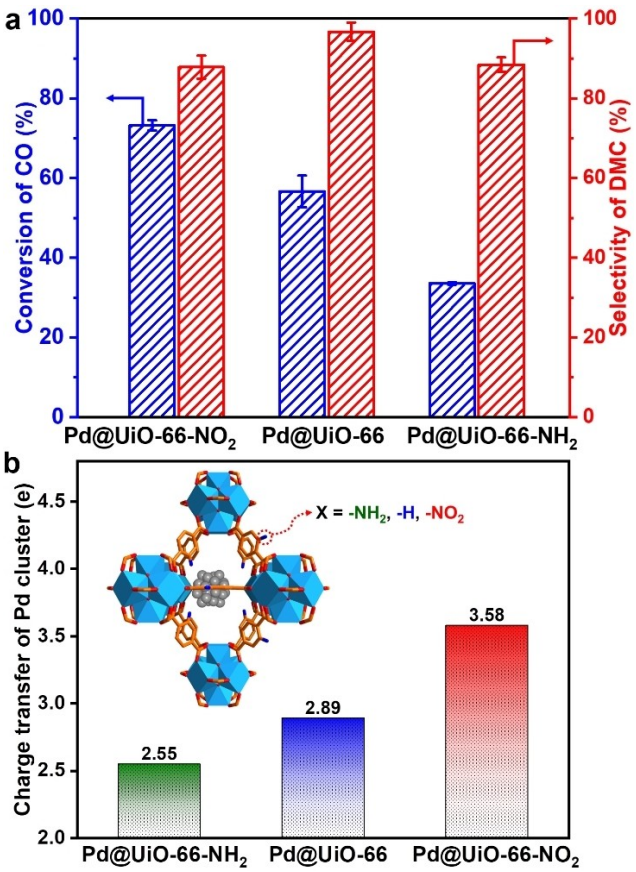


***Figure 5.*** a) The conversion and selectivity to DMC over Pd@UiO-66-X (X=-H, -$NO_2$, -$NH_2$) in the direct CO esterification under the reaction condition tending to produce DMC: 180 mg catalyst, 120 °C, 0.1 MPa, WHSV = 2500 L$kg_{cat.}^{-1}$ $h^{-1}$, reactant gases composed of 19% CO, 45% MN, 3% Ar, and 33% $N_2$. The selectivity and conversion are calculated based on CO. b) The calculated number of electron transfer from Pd clusters to the MOF in Pd@UiO-66-X.

calculated numbers of electron transfer from Pd clusters to UiO-66-$NO_2$, UiO-66, and UiO-66-$NH_2$ are 3.58, 2.89, and 2.55e, respectively (Figure 5b), indicating the Pd electron densities follow the order of Pd@UiO-66-$NO_2$ < Pd@UiO-66 < Pd@UiO-66-$NH_2$.[8a] To further illustrate the influence of different Pd electron densities on catalytic activity, DRIFT spectra of CO adsorption are adopted to detect the adsorption behavior of CO molecules on Pd@UiO-66-X (Figure S17). The main CO adsorption peaks of Pd@UiO-66-X fall into the range of 1900–2000 $cm^{-1}$, which are assigned to the C–O vibrations of bridged CO adsorption on Pd NPs.[14a] The similar adsorption mode of CO over the three samples implies that Pd NPs in Pd@UiO-66-X are of the same structure.[8a] The obvious red shift of the main CO adsorption peak for the three catalysts indicates that the Pd electron density follows the trend of Pd@UiO-66-$NH_2$ > Pd@UiO-66 > Pd@UiO-66-$NO_2$, which is in good agreement with the above calculated results. The relationship between the red shift of CO adsorption peaks and Pd electron density can be explained by that, when Pd NPs are electron-rich, more electrons are injected into the 2π* orbitals of CO (electron backdonation), giving rise to stronger Pd-CO adsorption and weakened C–O bond. Therefore, the electron density of Pd species is linearly correlated with CO adsorption intensity. Given that the strong adsorption of CO is not conducive to the direct CO esterification according to the previous reports,[14b] the above analyses can well explain the activity trend for Pd@UiO-66-X, highlighting that the activity of the CO esterification can be improved by rationally modulating the microenvironment and electron density of Pd NPs by pore wall functionalization of the MOF.

The stability investigation for Pd@UiO-66-X indicates that the catalytic activity and high DMC selectivity can be well maintained (Figure S18). The Pd@UiO-66 keeps the high selectivity to DMC (>95%) even extending the reaction time to 30 h (Figure S19). Powder XRD patterns and TEM observations for Pd@UiO-66-X after reaction suggest the retained MOF crystallinity and Pd sizes in the catalysis (Figures S20, S21). The similar XPS spectra of Pd@UiO-66-X before and after the CO esterification support that the existing form of Pd NPs in these samples could be maintained after reaction (Figure S22).

## Conclusion

In summary, Pd NPs of ~2 nm are encapsulated into UiO-66-X with different functional groups to afford Pd@UiO-66-X, which exhibits high selectivity to DMC (up to ~99%) in the direct CO esterification. This is an unprecedented finding for the CO esterification over Pd NPs that always gives high DMO selectivity in all previous reports, as also supported by Pd/UiO-66 with Pd NPs on the MOF particles in this work. Moreover, the Pd electron density can be rationally regulated based on microenvironment modulation by altering the MOF functional groups in Pd@UiO-66-X (X=-H, -$NO_2$, -$NH_2$), leading to optimized activity. Both experimental and DFT calculation results suggest that, microenvironment of Lewis acid site number surrounding Pd NPs, being associated with the interface level between Pd and Zr-oxo cluster, is found to play a critical role in the resulting selectivity, where abundant Lewis acid sites interfacially contacted with Pd NPs in Pd@UiO-66 are beneficial to high DMC selectivity, while Pd/UiO-66 with less interface and less Lewis acid sites surrounding Pd NPs, following a different reaction pathway, affords DMO product as always reported. This work not only provides significant insights into the optimized electronic state and activity of metal NPs by modulating their microenvironment, but also opens up a new avenue to selectivity regulation by controlling the location of active metal sites relative to porous supports in heterogeneous catalysis.

## Acknowledgements

This work was supported by the National Key Research and Development Program of China (2021YFA1500400, 2021YFB3801600, 2018YFA0704500), the Strategic Priority Research Program of the Chinese Academy of Sciences

(XDB0450302, XDA29030600), National Natural Science Foundation of China (22331009, U22A20401, 22172171, 22101269) and Fundamental Research Funds for the Central Universities (WK2060000038).

## Conflict of Interest

The authors declare no conflict of interest.

## Data Availability Statement

The data that support the findings of this study are available from the corresponding author upon reasonable request.

**Keywords:** Heterogeneous Catalysis · Lewis Acid Sites · Metal–Organic Frameworks · Microenvironment Modulation · Palladium

[1] a) Y. Liu, D. Deng, X. Bao, *Chem* **2020**, *6*, 2497–2514; b) Q. Zhang, J. Yu, A. Corma, *Adv. Mater.* **2020**, *32*, 2002927; c) W. Zhou, K. Cheng, J. Kang, C. Zhou, V. Subramanian, Q. Zhang, Y. Wang, *Chem. Soc. Rev.* **2019**, *48*, 3193–3228; d) X. Zhang, W. Huang, L. Yu, M. García-Melchor, D. Wang, L. Zhi, H. Zhang, *Carbon Energy* **2023**, https://doi.org/10.1002/cey2.362.

[2] a) H. Yue, Y. Zhao, X. Ma, J. Gong, *Chem. Soc. Rev.* **2012**, *41*, 4218–4244; b) G. Fiorani, A. Perosa, M. Selva, *Green Chem.* **2018**, *20*, 288–322; c) J. Zheng, L. Huang, C.-H. Cui, Z.-C. Chen, X.-F. Liu, X. Duan, X.-Y. Cao, T.-Z. Yang, H. Zhu, K. Shi, P. Du, S.-W. Ying, C.-F. Zhu, Y.-G. Yao, G.-C. Guo, Y. Yuan, S.-Y. Xie, L.-S. Zheng, *Science* **2022**, *376*, 288–292.

[3] a) S. Ji, Y. Chen, G. Zhao, Y. Wang, W. Sun, Z. Zhang, Y. Lu, D. Wang, *Appl. Catal. B* **2022**, *304*, 120922; b) Z.-Q. Wang, J. Sun, Z.-N. Xu, G.-C. Guo, *Nanoscale* **2020**, *12*, 20131–20140.

[4] R. Guo, Z. Hou, J. Chen, Y. Qin, G. Chai, Y. Yao, *Fuel* **2022**, *330*, 125484.

[5] a) S.-Y. Peng, Z.-N. Xu, Q.-S. Chen, Z.-Q. Wang, D.-M. Lv, J. Sun, Y. Chen, G.-C. Guo, *ACS Catal.* **2015**, *5*, 4410–4417; b) Z.-Y. Chi, L.-Q.-Q. Yang, X.-G. Li, Y.-L. He, W.-D. Xiao, *Chem. Eng. J.* **2022**, *446*, 136656; c) C. Wang, N. Xu, K. Huang, B. Liu, P. Zhang, G. Yang, H. Guo, P. Bai, S. Mintova, *Chem. Eng. J.* **2023**, *466*, 143136; d) L. Yang, Z. Pan, D. Wang, S. Wang, X. Wang, H. Ma, W. Qu, Z. Tian, *Catal. Sci. Technol.* **2023**, *13*, 3796–3803.

[6] a) H. Furukawa, K. E. Cordova, M. O'Keeffe, O. M. Yaghi, *Science* **2013**, *341*, 1230444; b) S. Horike, S. Kitagawa, *Nat. Mater.* **2022**, *21*, 983–985; c) M. Ding, R. W. Flaig, H.-L. Jiang, O. M. Yaghi, *Chem. Soc. Rev.* **2019**, *48*, 2783–2828; d) J. Liu, T. A. Goetjen, Q. Wang, J. G. Knapp, M. C. Wasson, Y. Yang, Z. H. Syed, M. Delferro, J. M. Notestein, O. K. Farha, J. T. Hupp, *Chem. Soc. Rev.* **2022**, *51*, 1045–1097; e) J. Gao, Q. Huang, Y. Wu, Y.-Q. Lan, B. Chen, *Adv. Energy Sustainability Res.* **2021**, *2*, 2100033; f) A. N. Hong, H. Yang, X. Bu, P. Feng, *EnergyChem* **2022**, *4*, 100080; g) Q.-J. Wu, J. Liang, Y.-B. Huang, R. Cao, *Acc. Chem. Res.* **2022**, *55*, 2978–2997; h) A. Ebadi Amooghin, H. Sanaeepur, R. Luque, H. Garcia, B. Chen, *Chem. Soc. Rev.* **2022**, *51*, 7427–7508.

[7] a) A. Aijaz, A. Karkamkar, Y. J. Choi, N. Tsumori, E. Rönnebro, T. Autrey, H. Shioyama, Q. Xu, *J. Am. Chem. Soc.* **2012**, *134*, 13926–13929; b) C. Fang, L. Liu, J. Weng, S. Zhang, X. Zhang, Z. Ren, Y. Shen, F. Meng, B. Zheng, S. Li, J. Wu, W. Shi, S. Lee, W. Zhang, F. Huo, *Angew. Chem. Int. Ed.* **2021**, *60*, 976–982; c) X. Li, T. Goh, L. Li, C. Xiao, Z. Guo, X. Zeng, W. Huang, *ACS Catal.* **2016**, *6*, 3461–3468; d) Q. Yang, Q. Xu, H.-L. Jiang, *Chem. Soc. Rev.* **2017**, *46*, 4774–4808; e) K. L. Kollmannsberger, L. Kronthaler, J. R. Jinschek, R. A. Fischer, *Chem. Soc. Rev.* **2022**, *51*, 9933–9959; f) M. Mukoyoshi, H. Kitagawa, *Chem. Commun.* **2022**, *58*, 10757–10767; g) J. Chen, Y. Wang, F. Wang, Y. Li, *Angew. Chem. Int. Ed.* **2023**, *62*, e202218115; h) G. Li, S. Zhao, Y. Zhang, Z. Tang, *Adv. Mater.* **2018**, *30*, 1800702.

[8] a) D. Chen, W. Yang, L. Jiao, L. Li, S.-H. Yu, H.-L. Jiang, *Adv. Mater.* **2020**, *32*, 2000041; b) L. Li, Z. Li, W. Yang, Y. Huang, G. Huang, Q. Guan, Y. Dong, J. Lu, S.-H. Yu, H.-L. Jiang, *Chem* **2021**, *7*, 686–698; c) M. Zhao, K. Yuan, Y. Wang, G. Li, J. Guo, L. Gu, W. Hu, H. Zhao, Z. Tang, *Nature* **2016**, *539*, 76–80; d) W. Zhang, W. Shi, W. Ji, H. Wu, Z. Gu, P. Wang, X. Li, P. Qin, J. Zhang, Y. Fan, T. Wu, Y. Fu, W. Zhang, F. Huo, *ACS Catal.* **2020**, *10*, 5805–5813; e) L. Jiao, J. Wang, H.-L. Jiang, *Acc. Mater. Res.* **2021**, *2*, 327–339; f) H. Wang, X. Liu, W. Yang, G. Mao, Z. Meng, Z. Wu, H.-L. Jiang, *J. Am. Chem. Soc.* **2022**, *144*, 22008–22017.

[9] a) J. H. Cavka, S. Jakobsen, U. Olsbye, N. Guillou, C. Lamberti, S. Bordiga, K. P. Lillerud, *J. Am. Chem. Soc.* **2008**, *130*, 13850–13851; b) S. Biswas, P. Van der Voort, *Eur. J. Inorg. Chem.* **2013**, 2154–2160.

[10] a) M. Xu, D. Li, K. Sun, L. Jiao, C. Xie, C. Ding, H.-L. Jiang, *Angew. Chem. Int. Ed.* **2021**, *60*, 16372–16376; b) K. Nikolaev, S. Ermakov, Y. Ermolenko, E. Averyaskina, A. Offenhäusser, Y. Mourzina, *Bioelectrochemistry* **2015**, *105*, 34–43.

[11] L.-L. Ling, W. Yang, P. Yan, M. Wang, H.-L. Jiang, *Angew. Chem. Int. Ed.* **2022**, *61*, e202116396.

[12] a) Y.-Z. Chen, B. Gu, T. Uchida, J. Liu, X. Liu, B.-J. Ye, Q. Xu, H.-L. Jiang, *Nat. Commun.* **2019**, *10*, 3462; b) M. Ding, H.-L. Jiang, *ACS Catal.* **2018**, *8*, 3194–3201.

[13] a) C. Wang, P. Chen, Y. Li, G. Zhao, Y. Liu, Y. Lu, *J. Catal.* **2016**, *344*, 173–183; b) H.-Z. Tan, Z.-N. Chen, Z.-N. Xu, J. Sun, Z.-Q. Wang, R. Si, W. Zhuang, G.-C. Guo, *ACS Catal.* **2019**, *9*, 3595–3603.

[14] a) C. Wang, L. Han, P. Chen, G. Zhao, Y. Liu, Y. Lu, *J. Catal.* **2016**, *337*, 145–156; b) Z.-N. Xu, J. Sun, C.-S. Lin, X.-M. Jiang, Q.-S. Chen, S.-Y. Peng, M.-S. Wang, G.-C. Guo, *ACS Catal.* **2013**, *3*, 118–122; c) S.-Y. Peng, Z.-N. Xu, Q.-S. Chen, Z.-Q. Wang, Y. Chen, D.-M. Lv, G. Lu, G.-C. Guo, *Catal. Sci. Technol.* **2014**, *4*, 1925–1930.

[15] a) Y. Dong, S. Huang, S. Wang, Y. Zhao, J. Gong, X. Ma, *ChemCatChem* **2013**, *5*, 2174–2177; b) C. Wang, W. Xu, Z. Qin, H. Guo, X. Liu, S. Mintova, *J. Energy Chem.* **2021**, *52*, 191–201; c) H.-Y. Wu, Y.-Y. Qin, Y.-H. Xiao, J.-S. Chen, R. Ye, R. Guo, Y.-G. Yao, *Small* **2023**, *19*, e2208238; d) H.-Y. Wu, Y.-Y. Qin, Y.-H. Xiao, J.-S. Chen, R. Guo, S.-Q. Wu, L. Zhang, J. Zhang, Y.-G. Yao, *Inorg. Chem. Front.* **2022**, *9*, 2379–2388.

[16] L. Liu, A. Corma, *Nat. Rev. Mater.* **2020**, *6*, 244–263.

[17] D.-M. Lv, Z.-N. Xu, S.-Y. Peng, Z.-Q. Wang, Q.-S. Chen, Y. Chen, G.-C. Guo, *Catal. Sci. Technol.* **2015**, *5*, 3333–3339.

Manuscript received: August 9, 2023
Accepted manuscript online: September 1, 2023
Version of record online: September 12, 2023